Effect of substrate and bond coat on contact damage in zirconia-based plasma-sprayed coatings

Sataporn Wuttiphan [a,1], Antonia Pajares [a,2], Brian R. Lawn [a,*], Christopher C. Berndt [b]

[a] *Materials Science and Engineering Laboratory, National Institute of Standards and Technology, Gaithersburg, MD 20899, USA*
[b] *Department of Materials Science and Engineering, State University of New York at Stony Brook, Stony Brook, NY 11794, USA*

Abstract

This paper reports a Hertzian indentation study of damage modes in zirconia-based plasma-sprayed coatings on metal substrates, with and without bond coats. The structure of the study is as follows: (i) measurement of Hertzian indentation stress–strain curves, first on individual bulk material components (controls) and then on the composite layer structures, to quantify the degree of plasticity; (ii) micrographic analysis of the corresponding subsurface damage modes, particularly of the yield zones, in both coatings and underlayers; (iii) finite element modelling of the elastic–plastic stress fields in the adjacent layers, again with a focus on the yield zones. It is demonstrated that the substrate can have a profound influence on the damage distribution, depending on the degree of elastic–plastic mismatch relative to the coating. The bond coat, by virtue of its relative thinness, plays a lesser role in the damage intensity, notwithstanding an apparent improvement in substrate adhesion. Indentation variables followed are applied load, to examine the evolution of damage, and number of cycles, to examine fatigue. The results indicate the power and simplicity of the Hertzian technique as a route to mechanical characterization of coating structures: for identifying damage modes, especially yield (but also fracture, in the present case delamination fracture); for evaluating damage parameters, such as Young's modulus and the yield stress, from FEM analysis of stress–strain curves and yield zone microscopy; and for quantifying design concepts, e.g. maximum sustainable bearing stress and damage tolerance.

Keywords: Bond coat; Coating; Contact damage; Delamination ; Indentation stress–strain curve; Plasticity; Substrates; Thermal spray coatings; Zirconia

1. Introduction

Plasma-spray ceramic coatings on metal alloy substrates have many applications, for thermal barrier protection, wear and corrosion resistance, enhanced biocompatibility in prosthetic devices, and so on [1–3]. Ultimate performance of the coating depends sensitively on the choice of substrate as well as the coating material itself, in addition to a myriad of thermal spray variables [4]. Bond coats add to the effectiveness of the ensuing structures, and afford extra adhesion of the overlying coating to the underlying substrate. Despite (or perhaps because of) their high defect contents, plasma-sprayed coating systems show uncommon damage tolerance, with impressive lifetime performance under most severe operating conditions. At the same time modes of failure, when

they do occur, have not been well characterized, especially in relation to material microstructures.

Recently, we have developed a Hertzian contact technique for investigating damage accumulation in plasma-sprayed structures [5–7]. Experimentally, the Hertzian test procedure is the essence of simplicity, requiring little more than a hard spherical indenter, a conventional mechanical testing machine, and routine microscopy facilities. Theoretical interpretation of the contact damage, on the other hand, is relatively complex, involving analysis of a highly nonlinear, inhomogeneous elastic–plastic field, usually by finite element modelling (FEM) [8]. Qualitatively, the method enables identification of intralayer and interlayer deformation and fracture damage modes, and tracks the evolution of these damage processes with increasing load or number of cycles. It is especially effective in mapping out subsurface "yield" zones beneath the contact. Such yield zones tend to be extensive in the metal substrate, where conventional dislocation-driven processes operate (plasticity); but they also occur to a limited extent in the ceramic coating, from the cumulative effect of microstructurally discrete shear faults ("quasi-plas-

---

* Corresponding author.
[1] This work represents part of a PhD dissertation, Department of Materials and Nuclear Engineering, University of Maryland, College Park, MD 20742, USA.
[2] Guest Scientist, from Departamento de Física, Universidad de Extremadura, 06071 Badajoz, Spain.

ticity'' [9]). Characteristic fracture patterns in the coating are also identifiable. Quantitatively, the method enables measurement of indentation stress–strain curves, indicating the relative amounts of elastic and plastic deformation. These stress–strain curves are useful for evaluating damage tolerance and for determining design stresses, and as such present a sensitive alternative to the more conventional load–displacement curves used in nano-indentation techniques [10].

In the present paper we analyze the results of a Hertzian contact study on a model plasma spray coating system. The broad aim of the study is to correlate experimental observations of the subsurface yield deformation within the coating and substrate with corresponding FEM simulations. A more specific aim is to demonstrate the potential role of the underlayers, bond coat as well as substrate, in the mechanical performance of the coating system. For this purpose a zirconia:yttria coating on both steel and nickel-based superalloy substrates, with and without a NiCrAlY bond coat, is chosen as our model system. Control tests on free-standing bulk specimens are used to ''calibrate'' the constituent elasticity and plasticity parameters for subsequent computations of the layer composite responses. We show how the substrate can strongly enhance or inhibit the contact yield zone, depending on the relative hardness, with corresponding modification of the indentation stress–strain curve. Conversely, we show that the presence of a bond coat has little effect on the ultimate yield zone geometry and stress–strain curve, presumably because of its relative thinness. Finally, the insensitivity of the coating damage to repeat loadings of the indenter, consistent with a fatigue-resistant, damage tolerant structure, is indicated.

2. Experimental

2.1. Materials selection and characterization

Ceramic coatings using starting powders of zirconia with 8 wt% yttria (Amdry 142, Amdry, Troy, MI) were air plasma-sprayed to a thickness of 300 ± 20 μm onto metal substrates. The substrates were at least 3 mm thick for adequate contact support and were grit-blasted for optimal adhe-

sion. Two substrate metals with widely different hardnesses were used: a soft steel, with and without 120 ± 20 μm Ni-CrAlY alloy (Ni-346-1, Union Carbide, Indianapolis, IN) bond coat; and a hard nickel-based superalloy (Inconel 601, Union Carbide, Indianapolis, IN) with the same bond coat. Some free-standing zirconia:yttria and bond coat specimens were sprayed to thicknesses of about 3 mm, and some metal blanks were set aside without coating, to provide bulk reference material states.

Selected specimens were sectioned and given a final polish with 1 μm diamond paste for characterization. Vickers indentation tests were carried out on each material component in these specimen sections to determine hardness values; these are listed in Table 1, along with other pertinent materials data. We note from the table that the coating is considerably harder than the steel substrate, and also the bond coat, but is softer than the superalloy. In the zirconia:yttria coating, no well-defined radial cracks were observed around the Vickers indents; rather, the indentations opened up pre-existing interlayer laminar microcracks, confirming the weakness of the laminate in the plasma-sprayed microstructure [5].

2.2. Hertzian indentation tests

Indentation stress–strain curves were determined on the polished top surfaces of layer and bulk material specimens using tungsten carbide spheres of specified radius [5,6]: on the layer structures, with a fixed radius $r = 3.18$ mm; and on the bulk control materials, with a broader range of radii, $r = 1.98$–12.7 mm, to allow for more accurate material parameter calibrations. Measurements of the contact radius a at each sphere radius r and load P were made at the impressions, to enable evaluations of indentation stress ($p_0 = P/\pi a^2$) as a function of indentation strain (a/r). (At low loads a thin gold coat deposited before indentation helped to demarcate the contact areas, from a residual flattening of the relatively soft film.) The critical contact pressure $p_Y \approx 1.1Y$ [11] for initiation of subsurface irreversible deformation in each bulk material was measured from contacts at which permanent impressions were first detected, to enable determination of the yield stresses Y. (In these experiments it was found advantageous to coat the surface after indentation, to enhance phase contrast in Nomarski illumination.)

Table 1

Elastic and yield parameters for the materials used in finite element modelling: E from the initial slope of indentation stress–strain data (ν from supplier specifications, or literature values); H directly from Vickers impressions (load/projected area); Y from critical contact pressure at first yield; α from best fits to the indentation stress–strain data

Material	Young's modulus, E (GPa)	Poisson's ratio, ν	Hardness, H (GPa)	Yield stress, Y (GPa)	Work-hardening coeff., α
Zirconia:yttria	34	0.26	3.5	0.70	0.80
NiCrAlY alloy	28	0.30	2.2	0.73	0.55
Steel [a]	210	0.30	1.2	0.39	0
Superalloy	192	0.25	4.3	0.85	0.12
Tungsten carbide [b]	614	0.22	19	6.0	0.25

[a] Ref. [18]

[b] Indenter. Refs. [19,20].

Some load–point-displacement tests were run on a coating/bond-coat/steel specimen, for comparison with the indentation stress–strain data. These tests were made using a crack-opening displacement clip gauge mounted at one end on the specimen surface and at the other on the base of the shaft housing the indenting sphere, and the results were analyzed using a data acquisition system.

Profile views of subsurface damage zones were obtained using bonded-interface specimens. Specimens were cut into halves, polished at the section faces, realigned, and re-mated; the last was achieved either by adhesive, in the case of the bulk materials [12], or by screws through the metal substrate base, in the case of the layer structures [5]. Lines of indentations were then made along the trace of the bonded interface on the top surface, using an indenter of radius $r = 3.18$ mm. Single-cycle tests were conducted at peak loads up to $P = 3000$ N. Multiple-cycle tests were conducted at a single low load, $P = 250$ N, at a frequency 10 Hz. The indented specimens were separated, cleaned and gold coated, and viewed optically in Nomarski interference contrast.

3. Finite element modelling

A commercial package (Strand, G and D Computing Pty. Ltd, Sydney, Australia) was used to perform finite element modelling (FEM) of the indentation configurations. The algorithm models an indenting sphere, radius $r = 3.18$ mm, in frictionless axisymmetric contact with an initially flat specimen $4 \times 4 \times 4$ mm. The calculations are performed for a coating thickness $d = 300$ μm and (where applicable) a bond coat thickness $h = 120$ μm [8]. Fig. 1 shows a portion of the cross-section mesh in the near-contact region. Strong interfacial bonding is assumed between the adjacent layers (no delamination). Contact is incremented monotonically to the peak load in 40 steps, with a maximum of 50 iterations at
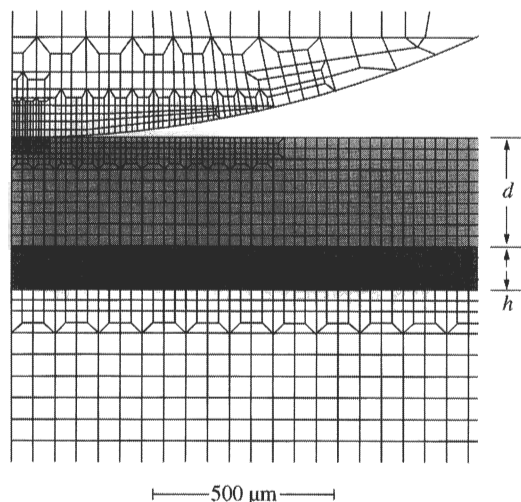

Fig. 1. Finite element model (FEM) mesh for indentation of coating with a bond coat on substrate, showing a portion of the half-section. The grid shown is for a sphere of radius $r = 3.18$ mm, coating thickness $d = 300$ μm and bond coat thickness $h = 120$ μm.

each increment and with tolerances 0.1% in force and 0.5% in displacement. At each load the contact radius a is determined, from which the stress–strain quantities $p_0 = P / \pi a^2$ and a / r are evaluated.

The algorithm has provision for input of constitutive uniaxial stress–strain responses $\sigma(\varepsilon)$ for each layer material, as well as for the indenter material [8]. It allows each material to deform according to a modified critical shear stress condition with linear strain hardening [13]:

$$\begin{aligned} \sigma &= E\varepsilon, & (\sigma < Y) \\ \sigma &= Y + \alpha(\varepsilon E - Y), & (\sigma > Y) \end{aligned} \qquad (1)$$

where E is Young's modulus, Y is the uniaxial compression stress for the onset of yield, and α is a dimensionless strain-hardening coefficient in the range $0 \le \alpha \le 1$ ($\alpha = 1$, fully elastic; $\alpha = 0$, fully plastic). The parameters in Eq. (1) therefore need to be "calibrated" in order to enable computations to be made for the layer structures.

Among other things, the FEM algorithm enables point-by-point evaluation of the principal stresses σ_1, σ_2 and σ_3 below the contact. Our primary interest lies in the maximum shear stress τ defined in the broader subsurface region by $\tau_{31} = \frac{1}{2}(\sigma_3 - \sigma_1)$, and in a shallow near-surface region outside the contact by $\tau_{12} = \frac{1}{2}(\sigma_1 - \sigma_2)$ [13].[3] We are expressly interested in the contour $\tau = Y/2$ that defines the boundary of yield zone.

In the present study we neglect potential complications from any superposed macroscopic residual stresses associated with coating/substrate thermal expansion mismatch, and from the post-contact residual field that inevitably drives coating/substrate delamination on unloading [8].

4. Results and analysis

4.1. Stress–strain curves

In this subsection we consider the indentation stress–strain curves for the various coating/substrate systems, in order to establish a basis for later analysis of the yield zone geometries.

We first plot the results for the individual free-standing coating, bond coat and substrate materials, in Fig. 2. The data points represent experimental determinations, and the solid curves FEM fits to these data. All materials exhibit a small initial elastic region, followed by a more substantial plastic or quasi-plastic region. The indentation data are used to calibrate the elastic and yield parameters for the constituent materials in Table 1: the Young's moduli E are determined directly from best fits in the initial linear region [5], the yield stresses Y independently from direct microscopic determinations of first permanent impressions at the indentation sites

---

[3] In the conventional Hertzian elastic field for homogeneous isotropic solids, $\sigma_1 \ge \sigma_2 \ge \sigma_3$ everywhere except in the free-surface region, where $\sigma_2 < \sigma_3 = 0$ [14].
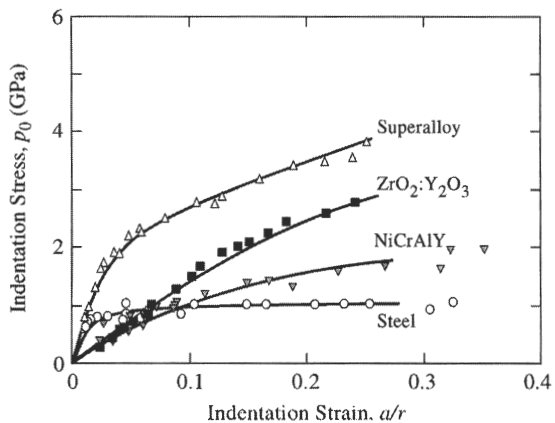
Fig. 2. Indentation stress–strain curve for free-standing materials, zirconia: yttria (coating), NiCrAlY alloy (bond coat), steel and superalloy (substrates). The data were obtained using a WC sphere, $r = 1.98–12.7$ mm (not distinguished). Solid curves: calibration FEM fits.

Fig. 4. Indentation stress–strain curve for zirconia:yttria coating, $d = 300$ μm, and a NiCrAlY bond coat, $h = 120$ μm, on a superalloy substrate. The data were obtained using a WC sphere, $r = 3.18$ mm. Solid curves: FEM predictions; dashed curves: individual coating and substrate materials from Fig. 2, which are included for comparison.

(Section 2), and the strain-hardening coefficients α from best fits in the nonlinear region [8]. Note that the curves for the zirconia:yttria and NiCrAlY fall well below that for the superalloy over the entire range of the stress–strain curve, and even below that for the soft steel in the low-strain region, attesting to the high defect content of the plasma-sprayed materials [4]. Indeed, the values of E for zirconia:yttria and NiCrAlY in Table 1 are an order of magnitude lower than the values for the corresponding fully dense bulk materials [5]. Deviations between the FEM-generated curves and experimental data amount to less than 10% in stress p_0 for any of the materials in Fig. 2 (although uncertainties in any one parameter may well exceed this level, especially in E, owing to the limited range of the elastic region in Fig. 2 [5]).

Indentation stress–strain results for the layered zirconia:yttria coating systems are shown in Figs. 3 and 4. Fig. 3 shows data for the coating with the steel substrate, with and without a bond coat; and Fig. 4 for the coating with the super-
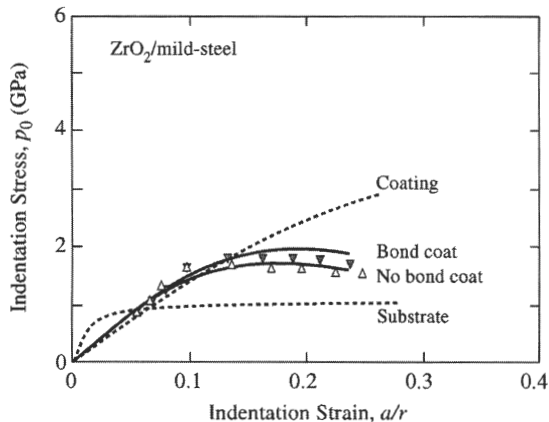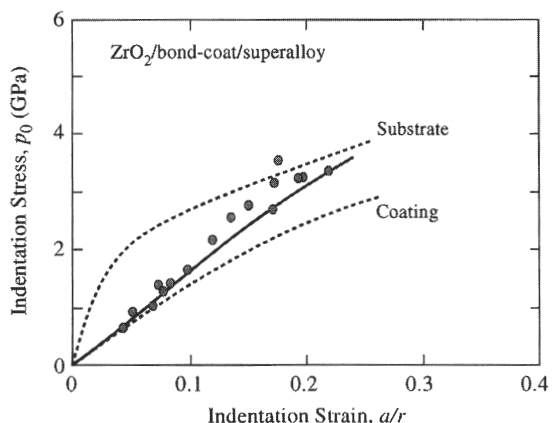
alloy substrate, with a bond coat. The solid curves are now a priori FEM predictions using the calibrated parameters in Table 1.[4] Deviations between the predicted curves and the data approach 20% in stress p_0 in these instances. The dashed curves are the FEM fits to the coating and substrate materials from Fig. 1. For the soft steel substrate in Fig. 3, the predictions for the composite layer structures more closely follow the coating curve at small strains, tending toward the substrate curve at large strains, with an intervening maximum [5]. The addition of a bond coat enhances this stress maximum in Fig. 3 slightly. An analogous asymptotic transition from the coating curve to the substrate curve is seen for the hard superalloy substrate in Fig. 4, but without the maximum. In this context, the mechanical role of the coating and bond coat may be regarded as "hardening" the steel substrate and "softening" the superalloy substrate, consistent with the relative hardness values in Table 1.

A conventional load–point-displacement trace for the zirconia:yttria/bond-coat/steel system is shown in Fig. 5, for comparison with the appropriate indentation stress–strain curve in Fig. 3. Hysteresis in the load–unload cycle is pronounced, consistent with the strong nonlinearity in the indentation stress–strain curve (the peak load $P = 3000$ N for the trace in Fig. 5 corresponds to the data point at extreme right in Fig. 3). Unlike the indentation stress–strain curve, however, the forward load–displacement trace provides no clear indication of the onset and development of the material plasticity (although the hysteresis does make it clear that plasticity has occurred); not even the location of the maximum (M) in Fig. 3, let alone the point of first substrate yield (Y), shows any discernable singularity in Fig. 5. The indentation stress–strain curve is therefore a far more sensitive indicator of the underlying material nonlinearity.

Fig. 3. Indentation stress–strain curve for zirconia:yttria coating, $d = 300$ μm, with and without a NiCrAlY alloy bond coat, $h = 120$ μm, on steel substrate. The data were obtained using a WC sphere, $r = 3.18$ mm. Solid curves: FEM predictions; dashed curves: individual coating and substrate materials from Fig. 2, which are included for comparison.

---

[4] For the layer materials under consideration here, the elastic limit of the relatively hard indenting sphere is never exceeded, so the plasticity parameters Y and α for WC in Table 1 are superfluous.
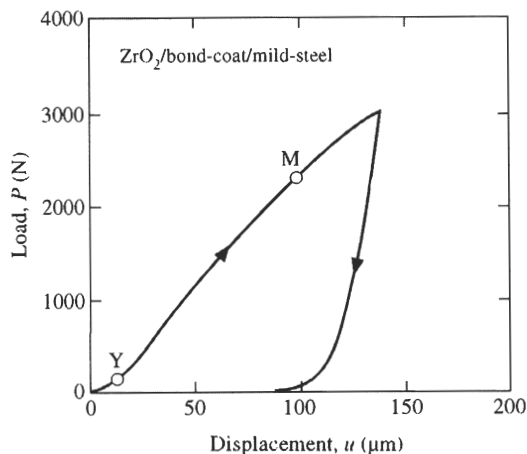
Fig. 5. Load–displacement curve for zirconia:yttria coating, $d = 300$ μm, with a NiCrAlY bond coat, $h = 120$ μm, on a steel substrate. The data were obtained for a WC sphere, $r = 3.18$ mm, $P = 3000$ N (corresponding to the highest-strain data point for the curve with a bond coat in Fig. 3). Point Y corresponds to the yield stress and M to the maximum in the appropriate indentation stress–strain curve in Fig. 3.

4.2. Contact damage modes

In this subsection we describe critical features of the sub-surface damage geometries at bonded-interface sections through the layer specimens, and compare these observations with predictions from the FEM stress analysis. Our primary focus will be on the dominant plasticity component of the damage, with secondary attention to accompanying fracture.

We begin with results for bulk free-standing zirconia:yttria in Fig. 6, to confirm that the ceramic component can indeed deform in a quasi-plastic mode [6,9,13]. Fig. 6 (top) shows a section micrograph from a bonded-interface specimen indented at peak load $P = 1500$ N, corresponding to an indentation strain $a/r = 0.15$ well into the plastic region (cf. Fig. 2). Subsurface damage, consisting of a distributed cloud of microstructural shear failures at interlaminar defects [5,6], is discernible immediately below the contact AA. In this material, however, the boundary of the damage zone is not clearly defined. This lack of definition may be attributable in part to the background porosity. Matters are compounded by an apparent gradient in damage density, peaking in concentration near the upper central regions of the damage zone and tapering off gradually toward the outer regions, a manifestation of the pronounced strain hardening in the underlying stress–strain response (large α in Table 1). Fig. 6 (bottom) designates the corresponding FEM-computed median-plane contours of the maximum principal shear stresses within the yield zone (Section 3). Stress levels are indicated by the degree of shading, to highlight the gradient. Notwithstanding the above uncertainties in locating the yield boundary, the FEM calculations appear to reproduce all the broader features of the zone shape and size, including the falloff in damage density toward the zone boundary.

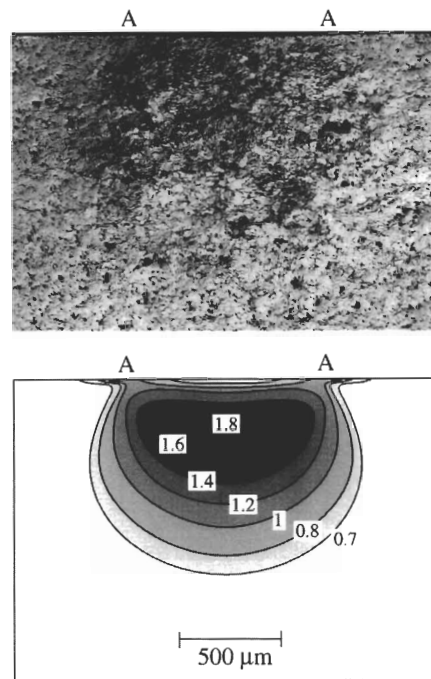Now consider the composite zirconia:yttria coating/underlayer systems. Fig. 7 shows section micrographs (top) and

Fig. 6. Contact damage in free-standing plasma-sprayed zirconia:yttria, from indentation with a WC sphere, $r = 3.18$ mm, $P = 1500$ N. Top: Nomarski micrograph of a section from a bonded-interface specimen. Bottom: corresponding FEM-computed shear stress contours within the yield zone (stresses in GPa), showing the field gradient (the lip in the FEM contour at the upper surface is due to the switch in principal stresses [13]). Contact diameter AA.

comparative FEM yield zone boundary predictions (bottom), for (a) coating/steel, (b) coating/bond-coat/steel, and (c) coating/bond-coat/superalloy, at a ''low'' load, $P = 500$ N; this load corresponds to an indentation strain $a/r \approx 0.10$, i.e. just within the nonlinear stress–strain region (cf. Fig. 3). For the coatings on steel (Fig. 7a,b), the yield zones in the substrate are well defined, characteristic of a soft metal with relatively small strain hardening (small α in Table 1). Limited yield is also evident in the ceramic coating and, in Fig. 7(b), in the intervening bond coat. For the coating on superalloy (Fig. 7c), no yield is evident in the substrate at this load, but some is observed in the coating and bond coat. Again, the FEM predictions appear to reproduce the broader features of the yield zone geometry.

Fig. 8 shows similar section micrographs (top) and comparative FEM yield zone predictions (bottom), but at a ''high'' load, $P = 1500$ N; this load corresponds to indentation strains well into the nonlinear region, $a/r \approx 0.16$ for the steel substrate and $a/r \approx 0.14$ for the superalloy substrate (cf. Fig. 3). In all cases shown, the substrate yield is considerably further developed relative to the lower load in Fig. 7, although again much more so in the steel in Fig. 8(a,b). The yield in the coating and bond coat is also considerably more intense, especially for the structure in Fig. 8(c), where it continues to eclipse that in the superalloy substrate.

To place the FEM predictions on a stronger quantitative footing, we plot in Fig. 9 the magnitude of principal shear
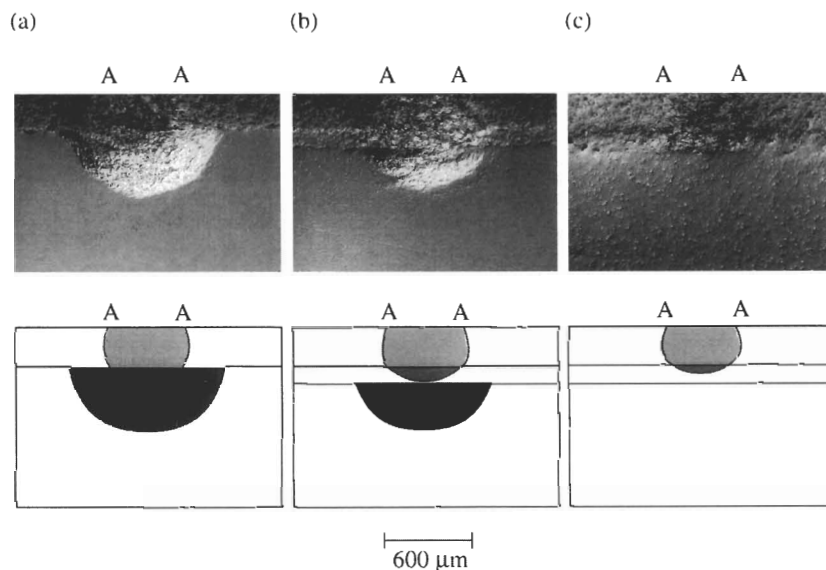
Fig. 7. Contact damage in zirconia:yttria coating (ZrO_2), $d = 300$ μm, with and without a NiCrAlY alloy bond coat (bc), $h = 120$ μm, on substrate: (a) ZrO_2/steel, (b) ZrO_2/bc/steel, (c) ZrO_2/bc/superalloy. Indentation with a WC sphere, $r = 3.18$ mm, $P = 500$ N. Top: Nomarski micrographs of sections from a bonded-interface specimen. Bottom: corresponding FEM-computed shear stress contours (stresses in GPa); the yield zones shaded. Contact diameter AA.
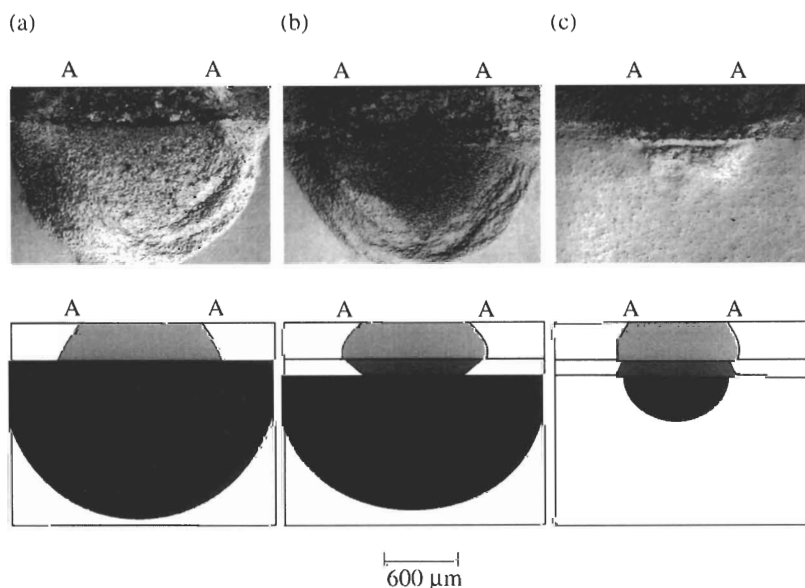

Fig. 8. Contact damage in zirconia:yttria coating (ZrO_2), $d = 300$ μm, with and without a NiCrAlY alloy bond coat (bc), $h = 120$ μm, on substrate: (a) ZrO_2/steel, (b) ZrO_2/bc/steel, and (c) ZrO_2/bc/superalloy. Indentation with a WC sphere, $r = 3.18$ mm, $P = 1500$ N. Top: Nomarski micrographs of sections from a bonded-interface specimen. Bottom: corresponding FEM-computed shear stress contours (stresses in GPa); the yield zones shaded. Contact diameter AA.

stress as function of depth along the contact axis, for the indentation conditions represented in Fig. 8. Data points in this plot are computed values at the FEM nodes, and the solid lines are smoothed curves through these points. Boundaries between coatings, bond coats and substrates are indicated. Vertical dashed lines indicate the yield stress levels within each material layer. The plots demonstrate how the stresses build up beneath the surface within the coating, and fall off in the bond coat and substrate. Fig. 9(a) compares the stress distributions for coatings with and without a bond coat on common steel substrates. The addition of the bond coat inten-

sifies the stress buildup in the coating, but the effect is slight because of the limited bond coat thickness. Similarly, Fig. 9(b) compares the distributions for coatings with a bond coat on steel and superalloy substrates. In this case the intensification of stress in the coating is much enhanced by replacement of the steel by the harder superalloy substrate.

Note in Fig. 6 that no cone fracture is apparent in the bulk coating material. In such quasi-plastic materials cone fracture is suppressed by a combination of redistribution of macroscopic tensile stresses and the deflection of any incipient surface ring cracks by the weak microstructural interfaces
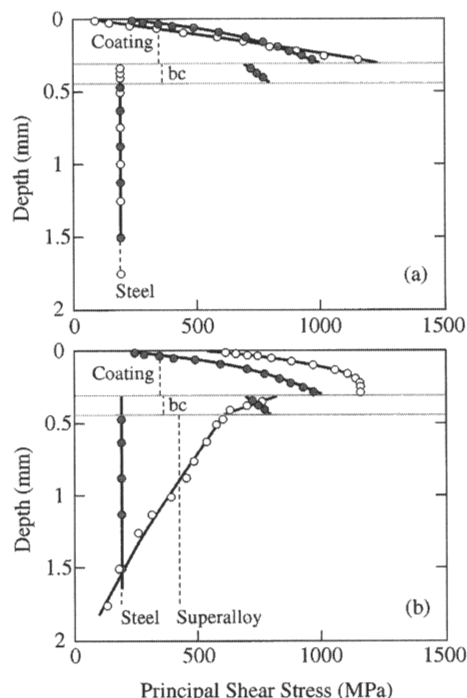
Fig. 9. Plots of maximum principal shear stress (τ_{31}) along the contact axis as function of depth in zirconia:yttria coating structures, for indentation with a WC sphere, $r = 3.18$ mm, $P = 1500$ N (cf. Fig. 8). Comparison of results for: (a) coatings with (filled circles) and without (open circles) a bond coat on steel substrates; (b) coatings with a bond coat on steel (filled circles) and superalloy (open circles) substrates. Data points: node stresses from the FEM calculations; solid curves: smoothed fits to the data.

Fig. 10. Higher-magnification views of delamination damage in (a) ZrO$_2$/steel, (b) ZrO$_2$/bc/steel, (c) ZrO$_2$/bc/superalloy. Indentation with a WC sphere, $r = 3.18$ mm, $P = 1500$ N (from Fig. 8).

[13]. Nor are cone fractures apparent in the coating structures in Figs. 7 and 8, contrary to observations in some laminate systems where flexural components in the stress state concentrate tension at the free surface outside the contact [6,15]. In the present zirconia:yttria coating structures, such fractures are presumably suppressed by the overriding predisposition to preferred microfailure along the discrete laminar weaknesses (Section 2.1) [5,6].

On the other hand, pronounced macroscopic interfacial delamination is evident at or near the interface of the coating with the immediate underlayer, substrate or bond coat, especially in Fig. 8. To see this delamination even more clearly, we show enlarged micrographs of these interfacial regions in Fig. 10. For the coatings with steel substrates (Fig. 10a,b), the delamination is especially large, reflecting strong residual elastic–plastic mismatch stresses between the steel and the other material components. The presence of the bond coat appears to have little influence on the delamination crack in the coating [5]; the bond coat itself remains intact, and maintains good bonding with the substrate. For the coatings with superalloy substrate (Fig. 10c), the delamination is comparatively minor, consisting of an incipient coalescence of laminar microcracks rather than a fully developed macrocrack within the actual coating rather than at the interface, reflecting smaller elastic/plastic mismatch stresses.
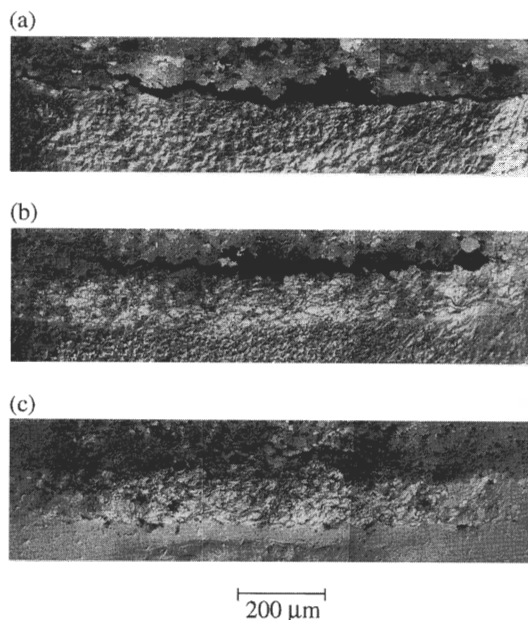
Micrographs of contact fatigue damage in each coating system for cyclic tests at $n = 1$, 10^3 and 10^5 cycles at a "very low" load $P = 250$ N (one-half the load used Fig. 7) are shown in Fig. 11. At this load, the system with the steel substrate but no bond coat in Fig. 11(a) shows a substrate yield zone after the first cycle. This substrate yield zone expands considerably with increasing cycles in Fig. 11(a). No such substrate yield is evident at any stage of cycling in either of the other two systems, not even in the system in Fig. 11(b) with the same steel substrate but with a bond coat. In this latter case, the interposed bond coat appears to have absorbed energy from the applied loading. At the same time, the damage in the coating intensifies in all three systems. In Fig. 11(a), and to a lesser extent in Fig. 11(b), this intensification is severe enough to suggest the beginnings of delamination failure at the coating/underlayer interface. For the system with the low-mismatch superalloy substrate in Fig. 11(c), the damage accumulation is relatively slight, although even in this case there are signs of incipient microcrack coalescence.

5. Discussion

The present study demonstrates the capacity of the Hertzian contact test as a means for characterizing damage modes in plasma-sprayed ceramic coatings on metal substrates. The test itself is experimentally simple and functionally powerful: it provides a measure of the intrinsic stress–strain behavior of the composite layer structure, in terms of individual material components; it facilitates identification of potential
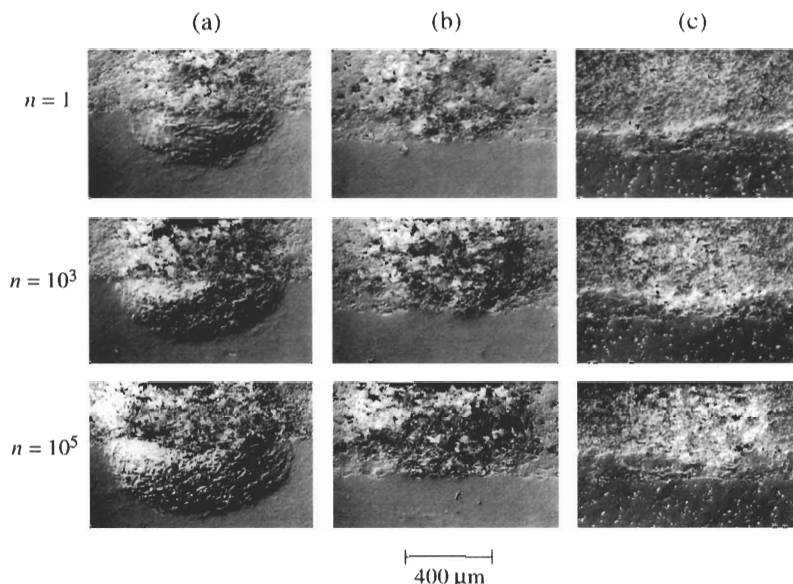
Fig. 11. Contact fatigue damage in zirconia:yttria coating (ZrO$_2$), $d = 300$ μm, with and without an NiCrAlY alloy bond coat (bc), $h = 120$ μm, on substrate: (a) ZrO$_2$/steel, (b) ZrO$_2$/bc/steel, (c) ZrO$_2$/bc/superalloy. Indentation with a WC sphere, $r = 3.18$ mm, $P = 250$ N, frequency 10 Hz, for $n = 1$, 10^3 and 10^5 Nomarski micrographs of sections from bonded-interface specimens.

sources of failure at internal weaknesses; and it enables tracking of damage evolution in the different layers under varied loading and fatigue conditions. In addition, the test is amenable to quantitative analysis using finite element modelling (FEM) or other analytical tools, with the ultimate promise of materials evaluation and design.

The indentation stress–strain response is especially instructive in the way it demonstrates how first the coating and then the substrate dominates the load-bearing capacity in a given contact. For the coating system with a relatively soft steel substrate (Fig. 3), the curve shows a characteristic maximum, marking a transition in load transfer from coating to substrate [5,6]; this maximum is modified only slightly by the inclusion of a thin bond coat. For the system with a hard superalloy substrate (Fig. 4), no maximum exists at all, and the stress increases monotonically with strain. Such curves thus provide distinctive indications of the relative roles of coating, bond coat, and substrate materials.

It is interesting to compare the indentation stress–strain curves with more conventional load–point-displacement curves obtained using instrumented indentation, specifically the upper solid curve in Fig. 3 with the loading curve in Fig. 5. It is apparent that the indentation stress–strain curve is much more dramatic in its revelation of nonlinear effects. Not even the existence of the highly distinctive maximum in Fig. 3 can be inferred from Fig. 5. The load–displacement curve is relatively insensitive to the underlying stress–strain nonlinearities. Of course, in weighing the practicality of load–displacement testing one needs to balance this lack of sensitivity against the comparative economy of data accumulation (a single indentation produces the entire curve in Fig. 5, just one data point in Fig. 3), along with the added energy information gained from the hysteresis in the full loading/unloading cycle.

New information can be gained about inherent damage modes in the coating structures from the microscopy, especially using the bonded-interface technique. In the micrographs in Figs. 7 and 8, for instance, the yield is seen to be particularly extensive in the structure with the soft steel substrate, and less so in the structure with the superalloy substrate. Yield occurs in the coating and bond coat as well as in the underlying metal. The bonded-interface sectioning method is especially useful in the simple way it identifies potential sources of failure. In the present zirconia-based coating systems, with their inbuilt laminar anisotropy, the most prevalent mode of failure in the coating is by interlaminate cracking, most clearly shown in Fig. 10. This tendency to interlaminate failure is consistent with observations from the exploratory Vickers indentations on section faces (Section 2.1) and from previous observations of failure modes in coatings with highly defective intralayers [5,6]. In this context, we note that no transverse cracks typical of more isotropic coating structures [6,16] are observed here. Accordingly, the section microscopy is effective in elucidating the role of microstructure in the damage characterization.

As indicated, the contact-induced damage has been quantified by FEM using a previously reported algorithm [8]. Given indentation stress–strain data from control tests on free-standing specimens, we first evaluate essential elastic–plastic parameters for each material component. Then we generate a priori stress–strain curves for a given layer structure for comparison with the corresponding experimental data, to demonstrate predictive capability. Once agreement between predicted and measured curves is deemed "accept-

able'' we can use the results from the FEM calculations to map out the entire contact stress field at any prescribed contact loading condition. Specific consideration of the principal shear stresses enables us to map out the yield zones in Figs. 6-8, for direct comparison with the yield zones in the corresponding micrographic images. This mapping may, in principle, be extended to the principal tensile stresses [8,13], for analysis of transverse brittle cracks in isotropic coating structures [16]; or, in the event the FEM algorithm is ultimately extended to the unloading half-cycle, for analysis of delamination.

The above results confirm the importance of elastic–plastic mismatch as a critical factor in the contact damage (Table 1, Fig. 2). Thus, yield and fracture (delamination) are greater in those coatings with the steel than with the superalloy substrate. In the latter case, the harder substrate substantially enhances the stress concentration (Fig. 9(b)). This enhanced concentration is more than compensated in the superalloy substrate by the relatively high yield stress (Table 1), with a consequent reduction in the size of the substrate plastic zone (Figs. 7 and 8); the same enhancement is, however, responsible for an increased damage intensity in the zirconia:yttria coating. Incorporation of the bond coat, on the other hand, has a comparatively minor influence on the stress–strain response (Fig. 9(a)), principally because of its relative thinness [17]; nor does the bond coat eliminate delamination in the coating (Fig. 10), despite any improvement in substrate adhesion.[5]

Finally, a brief word on the design consequences of the Hertzian test methodology. Indentation stress–strain curves provide a useful indication of the stresses that coatings may withstand in damage accumulation from spurious bearing or impact loads. The maximum in the stress–strain curves for zirconia:yttria coatings with steel substrates measures an upper deliverable stress intensity for the given layer system with a given indenter, regardless how high the load. Likewise, the exaggerated ''tail'' on these same stress–strain curves serves as an indicator of damage tolerance, i.e. the capacity of the system to sustain high strain at specified applied stress. Micrographic examinations of the damage regions offer the prospect of determining the extent to which elastic–plastic mismatch influences yield, fracture and (in cyclic loading) fatigue.

6. Conclusions

(i) Hertzian indentation testing has been conducted on model plasma-sprayed zirconia-based ceramic coatings on (soft) steel and (hard) superalloy substrates, with and without a bond coat. The test is advocated as a simple but powerful route to generic mechanical characterization of coatings.

---

[5] Of course, the bond coat is included not just to improve adhesion, but also (and sometimes more importantly) for corrosion protection.

(ii) Deformation modes in the ceramic coating and metal underlayer have been identified, using a bonded-interface section technique for observing subsurface contact damage. The metal substrate, depending on its relative hardness, can take up much of the load-bearing capacity by yielding in the sub-contact zone. The ceramic coating also shows limited yield (quasi-plasticity), accounting for damage tolerance in severe contacts and in repeated loading.

(iii) The damage in the zirconia-based coating systems has been quantified by indentation stress–strain curves, i.e. plots of indentation stress (contact load/area) against indentation strain (contact/sphere radius). For steel substrates, the curves pass through a maximum, signifying progressive load transfer from coating to substrate and indicating an upper limit to load-bearing capacity. For superalloy substrates, the curves increase monotonically, indicating an ever-increasing rigidity with penetration. Thin bond coats have only a minor modifying influence. The stress–strain curves are argued to be more sensitive indicators of underlying deformation processes than load–displacement curves from conventional instrumented indentation tests.

(iv) An elastic–plastic stress analysis of the damage has been carried out using finite element modelling (FEM). Control data from tests on bulk free-standing components provide essential material parameters for a priori computations for the coating structures. Indentation stress–strain functions generated in this way account for all the main features of the measured curves, and provide the basis for determining critical shear and tensile stress distributions for yield and (where applicable) fracture analysis.

References

[1] H. Herman, *Sci. Am., 256* (1988) 113.
[2] H. Herman, *Mater. Res. Soc. Bull., 13* (1988) 60.
[3] H. Herman, C.C. Berndt and H. Wang, in J.B. Wachtman and R.A. Haber (eds.) *Ceramic Films and Coatings*, Noyes Publications, Park Ridge, NJ, 1993, p. 131.
[4] L. Pawlowski, *The Science and Engineering of Thermal Spray Coatings*, Wiley, New York, 1995.
[5] A. Pajares, L. Wei, B.R. Lawn, N.P. Padture and C.C. Berndt, *Mater. Sci. Eng. A, 208* (1996) 158.
[6] A. Pajares, L. Wei, B.R. Lawn and C.C. Berndt, *J. Am. Ceram. Soc., 79* (1996) 1907.
[7] L. Wei, A. Pajares and B.R. Lawn, *J. Mater. Res., 11* (1996) 1329.

[8] A.C. Fischer-Cripps, B.R. Lawn, A. Pajares and L. Wei, *J. Am. Ceram. Soc., 79* (1996) 2619.

[9] B.R. Lawn, N.P. Padture, H. Cai and F. Guiberteau, *Science, 263* (1994) 1114.

[10] M.V. Swain and J. Mencik, *Thin Solid Films, 253* (1994) 204.

[11] D. Tabor, *Hardness of Metals*, Clarendon Press, Oxford, 1951.

[12] F. Guiberteau, N.P. Padture and B.R. Lawn, *J. Am. Ceram. Soc., 77* (1994) 1825.

[13] A.C. Fischer-Cripps and B.R. Lawn, *J. Am. Ceram. Soc., 79* (1996) 2609.

[14] F.C. Frank and B.R. Lawn, *Proc. Roy. Soc. Lond. A, 299* (1967) 291.

[15] H. Liu, B.R. Lawn and S.M. Hsu, *J. Am. Ceram. Soc., 79* (1996) 1009.

[16] K.S. Lee, S. Wuttiphan, X.Z. Hu, S.K. Lee and B.R. Lawn, *J. Am. Ceram. Soc.*, in press.

[17] M.C. Shaw, D.B. Marshall, M.S. Dadkhah and A.G. Evans, *Acta Metall., 41* (1993) 3311.

[18] A.C. Fischer-Cripps, *J. Mater. Sci.*, in press.

[19] H. Cai, M.A. Stevens Kalceff and B.R. Lawn, *J. Mater. Res., 9* (1994) 762.

[20] H. Cai, M.A.S. Kalceff, B.M. Hooks, B.R. Lawn and K. Chyung, *J. Mater. Res., 9* (1994) 2654.